Effects of K adsorption on the CO-induced restructuring of Co(11-20)

Marie Døvre Strømsheim[1], Ingeborg-Helene Svenum[2], Mari Helene Farstad[1], Zheshen Li[3], Ljubisa Gavrilovic[1], Xiaoyang Guo[1], Stine Lervold[1], Anne Borg[4], Hilde J. Venvik[1*]

[1]Department of Chemical Engineering, Norwegian University of Science and Technology (NTNU), 7491, Trondheim
[2]SINTEF Materials and Chemistry
[3]Department of Physics and Astronomy, ISA, Centre for Storage Ring Facilities, Aarhus Univerisity, 8000 Aarhus
[4]Department of Physics, Norwegian University of Science and Technology (NTNU), 7491, Trondheim

Corresponding author: hilde.j.venvik@ntnu.no

Abstract

The location of potassium (K) on Cobalt (Co) and its effect on adsorption and adsorption-induced surface restructuring is important for understanding the deactivation of Co Fischer-Tropsch catalysts and the nature of the active surface. Co(11-20) restructures by anisotropic migration of Co atoms upon CO exposure. Deposition of sub-monolayer amounts of K on Co(11-20) and the effect on the CO-induced restructuring were therefore investigated using scanning tunneling microscopy (STM), high resolution photoemission spectroscopy (HR-PES), and density functional theory calculations (DFT). The combined STM and DFT results suggest that the preferred adsorption site for K at low coverage is in the vicinity of step edges. DFT also found that diffusion of K along the [0001] direction, in between the zigzag rows of the topmost Co layer is facile. The restructuring under CO exposure with K pre-adsorbed proceeded on the terraces rather than from the step edges, in a slower and more disordered manner. HR-PES showed that the amount of CO adsorbed at saturation significantly decreased with predeposited K. The obstructed migration of Co atoms across the surface may be important in understanding why very low amounts of K on supported Co catalysts significantly reduces the activity towards hydrogenation of CO.

Keywords: Co single crystal, scanning tunneling microscopy, potassium, carbon monoxide, density functional theory, high resolution photoemission spectroscopy

Highlights

- CO adsorption on Co(11-20) with K predeposited studied by STM, HR-PES and DFT.
- Model system for the effect of K on Co based Fischer Tropsch catalysts.
- STM/DFT indicate that potassium is located near the step edges for low coverages.
- CO induced migration of Co is obstructed when potassium is present on the surface.
- The K-inhibited restructuring yielded less CO adsorbed.

1. Introduction

The presence of alkali or alkaline earth metals on the surface of a catalytically active metal may affect the catalyst activity, selectivity or stability in various ways, from enhancing the activity, suppressing deactivation or by-product formation, to acting as poisons. In the case that small amounts of alkali lead to extensive deactivation, it may be inferred that they affect the most active sites, such as is often the case for sulphur [1–3]. Understanding the effect hence becomes critical to eventual countering measures, but will also give information on the catalyst characteristics critical to its performance. Investigations of single crystal catalyst model systems have been important in this respect.

In the Fischer–Tropsch synthesis (FTS) [4], synthesis gas (CO, CO_2 and H_2) derived from natural gas, coal or biomass feedstocks is converted to hydrocarbon products, with cobalt (Co) or iron (Fe) based catalysts being the industrially relevant systems for this process. Alkali and alkaline earth species can be introduced to these catalysts through impurities in the synthesis gas, in particular when derived from biomass [5], in addition to being possible contaminants in the catalyst precursors. Co based catalysts are usually preferred in modern, natural gas based FTS technology [6], for which Li, Na, K, and Ca have been found to act as poisons [7,8]. For iron-based FTS, on the other hand, potassium (K) is utilized as a promotor, signifying the different states of the two catalysts under reaction conditions; i.e., metallic for Co and carbidic for Fe [9]. Impregnation of 20wt%Co/0.5wt%Re/γ-Al_2O_3-supported catalysts with alkali impurity loadings from 25 to 200 ppmw resulted in a significant decrease in catalyst activity during FTS [7,10]. It was therefore suggested that the adsorbed alkali metals were located in catalytically important sites. The H_2 chemisorption properties [7,10] and the H_2 and CO differential heats of adsorption [11], however, remained unaffected. Noting also

that the C_{5+} selectivity was maintained or slightly increased, reactant activation appears more affected than the subsequent chain growth steps.

Besides site blockage, the presence of impurities on the surface under reaction can induce changes to the surface morphology, as well as the inhibition of the dynamic restructuring of the surfaces/particles in response to the reaction conditions, resulting in changes in activity. In 2002, dynamic restructuring of supported Cu nanocrystals upon change of gaseous atmosphere was demonstrated by researchers at Haldor Topsøe A/S using in-situ transmission electron microscopy (TEM) [12]. More recently, dynamic morphological changes of the surface of Pt nanoparticles were shown to coincide with periodic variations in the reaction conditions for CO oxidation (1.0 bar of $CO:O_2$:He at 3:42:55 and 659K) [13]. Restructuring of the surface of the Co particles during the FTS reaction has also been discussed as a possible influence on catalyst behavior [14–20]. Evidence of Co particle restructuring was obtained by small-angle X-ray scattering (SAXS) investigations of Re-promoted Co-nanoparticles supported on γ-alumina under FTS conditions [18]. The change in surface structure upon introduction of synthesis gas was suggested to be caused by the migration of Co surface atoms. De Groot and Wilson [14] performed an early ex situ STM study of the Co(0001) surface after exposure to CO hydrogenation conditions (total pressure 4 bar, H_2:CO=2, 523 K). They reported a restructuring of the surface into triangular shaped Co islands, formed through a proposed migration of mobile cobalt carbonyl species. Recent in situ STM investigations of the Co(0001) surface under realistic FTS conditions (3 bar, H_2:CO=2, 483 K) also found a restructuring of the surface, with the formation of triangular Co nanoislands [19]. However, under the methanation limit condition of the FTS (14 mbar, H_2:CO=40, 493 K) an in situ high temperature high pressure STM investigation of a Co(0001) single crystal showed no morphological changes to the surface during the reaction [17]. Addition of <0.5 ppm sulphur to this synthesis gas, nevertheless, led to significant

changes in the surface morphology, through a combination of roughening and ordered superstructures [21].

Restructuring of Co(11-20) [22] and Co(10-12) [23] upon exposure to CO has previously been reported by our group during STM investigations under UHV conditions and room temperature. CO exposure gives a (3x1) reconstruction of these surfaces, as long known from LEED [24]. The STM observations revealed a restructuring process that could only be explained by extensive migration of Co across the surface. The nature of the migrating species could, however, not be determined and was suggested as single atoms, clusters or carbonyl-species. The migration was highly anisotropic, with troughs developing from the step edges along the row structure of the surfaces. The migrating material therefore resulted in the formation of ridges from the step edge, developing along the [0001] or [1010] direction for Co(11-20) and Co(10-12), respectively, to eventually meet a trough advancing from the adjacent (lower) step edge. The diffusion of Co species yielded the (3x1) structure in the case of (11-20) [22]. For (10-12), the migration was associated with the onset of a (1x2) structure that was neither observable nor previously reported from LEED, co-existing with an overlayer type (3x1) structure at saturation [23].

The deposition of alkali on Co single model systems and its effect on FTS-relevant adsorbates has so far only been investigated on Co(0001) [25–28] and Co(10-10) [29–31]. No surfaces where migration of Co atoms occurs during CO exposure have, to our knowledge, been investigated with respect to the influence of alkali adsorbates. Co(11-20) is therefore an appropriate model system to link the effect of adsorbed alkali metal to the possible restructuring occurring under FTS conditions. In this work, we report on the deposition of sub-monolayer amounts of potassium on the surface of Co(11-20) and the effect on CO adsorption, combining scanning tunneling microscopy (STM), high resolution photoemission spectroscopy (HR-PES), and density functional theory (DFT) calculations.

2. Materials and Methods

The Co(11-20) single crystal was cleaned by argon (purity 6.0) sputtering at 0.5-1 keV at room temperature (RT), and subsequent annealing at 600-630 K. The temperature was kept well below 700 K in order to avoid the phase transition from hcp to fcc structure in Co. A high number of cleaning cycles was necessary to obtain a clean surface, with annealing periods of several hours required to achieve a low degree of surface roughness. The cleaning process also involved a few exposures of the surface to oxygen (purity 6.0), followed by cycles of sputtering and annealing.

STM experiments were performed in an ultra-high vacuum (UHV) chamber, with a base pressure < $5x10^{-10}$ mbar. The UHV chamber contained an RT STM1 and low energy electron diffraction (LEED) optics from Omicron. All measurements were performed under UHV conditions and at RT. The long range order of the surface was checked with LEED prior to the STM experiments. Submomolayer amounts of K were deposited from a thoroughly degassed K-dispenser (SAES Getters). STM images were recorded during exposure to CO (purity 4.7) at pressures in the range $1\text{-}3\cdot10^{-9}$ mbar for the clean surface and with predeposited K. CO exposures are reported in Langmuir ($1L = 1.33\cdot10^{-6}$mbar·s). The tunneling currents and sample bias voltages used to acquire the STM images are specified in the figure captions. Background corrections of the STM images have been applied using the open source SPM program Gwyddion [32]. Distortion corrections have been applied to selected images, as stated in the figure captions.

HR-PES was performed at the MATLINE beamline of the ASTRID2 synchrotron facility in Aarhus, Denmark. The clean surface and the surface after submonolayer amounts of deposited K were exposed to CO beyond saturation levels (4-6 L). The Co 3p and O 1s core level spectra were recorded at photon energies 130 eV and 610 eV, respectively, while the C 1s and K 2p core level spectra were both recorded at 370 eV photon energy. All spectra were measured at normal emission. The binding energy was calibrated by recording the Fermi edge immediately after measuring a core level spectrum. Shirley background subtraction [33] and Voigt line shape were applied for fitting the C 1s core levels. Linear background subtraction and Doniach-Sunjic line shapes [34] were utilized in the fitting procedures for the K 2p core levels. The amount of K present on the surface was estimated from the cross section corrected area of the K $2p_{3/2}$ peak and the Co 3p peak of the clean surface after Shirley background subtraction.

DFT calculations were performed with the Vienna Ab Initio Simulation Package (VASP), with plane wave basis sets and pseudo-potentials [35]. The general gradient approximation (GGA) with the Perdew-Burke-Ernzerhof (PBE) functional [36] was applied for the exchange-correlation effect. The kinetic energy cut-off for the plane wave basis sets was 500 eV. The PAW pseudopotential [37,38] K_sv was utilized for potassium. The calculated lattice constants of hcp Co were a = 2.48 Å, and c = 4.04 Å, as compared to the experimental values a = 2.51 Å and c = 4.07 Å [39]. The clean Co(11-20) surface is illlustrated in Figure 1, and is made up by zigzag rows along the [0001] direction in alternating layers represented by layer A and B Co atoms. The surface was modelled by a periodically repeated slab consisting of six layers in total, separated by a vacuum region of about 17 Å. The bottom two layers were kept fixed and consistent with their bulk configurations, and the remaining layers were allowed to relax. Structural optimizations were performed with the shape and volume of the cell kept constant, but without constraints for the ionic positions and stress tensors.

Calculations were considered converged if all forces between the atoms were smaller than 0.01 eV/Å. Adsorption of K on Co(11-20) was investigated using (3x2) and (3x4) surface unit cells. Reciprocal space integration over the Brillouin zone was performed applying a finite sampling of a Γ-centered grid applying the Monkhorst-Pack scheme [40,41] of 3x5x1 and 3x3x1 k-points for the (3x2) and (3x4) surface unit cell, respectively. Adsorption was investigated by initially placing the adsorbate above high symmetry sites. As specified in Figure 1a there are six high symmetry sites: t_A, t_B, b_A, b_B, $b_{AB(1)}$ and $b_{AB(2)}$. The coverage in monolayers (ML) was defined as the number of adsorbates per surface atom in the topmost layers (layer A and B). Adsorption of K in association with a step edge was calculated by placing the K adatom above high symmetry sites on a (3x4) model surface cell with additional Co atoms placed above layer B. Adsorption energies for K on Co(11-20) were calculated as $E_{ads,K} = (1/n)[E_{surface,K} - (E_{clean} + nE_K)]$, with the terms being: $E_{surface,K}$ the total energy of the surface with K, E_{clean} the total energy of the clean Co surface, E_K the total energy of K, and n the number of K-atoms. In the case of CO adsorption, the adsorption energy without and with predeposited K was calculated by $E_{ads,CO} = E_{surface,CO} - (E_{surface} + E_{CO})$, where $E_{surface,CO}$ is the total energy of the system, $E_{surface}$ is the total energy of the surface without or with pre-adsorbed K, and E_{CO} the total energy of an isolated CO molecule. Negative adsorption energies indicate that adsorption is favorable. The reported adsorption energies are corrected for the zero point energy. The normal mode harmonic frequencies were calculated with the Co atoms kept fixed, and CO and K allowed to displace by 0.015 Å. The effective radius for K (R_{eff}) was calculated by the difference between the nearest neighbor K-Co distance and the effective radius of Co, $R_{eff} = (d_{K\text{-}Co} - a/2)$, where a is the calculated shorter lattice constant of hcp Co. Diffusion barriers were calculated using the Nudged Elastic Band (NEB) method [42]. Normal mode harmonic frequencies were calculated for the

transition states isolated with NEB, as well as the adsorption geometries. The transition state was verified by calculating the normal mode harmonic frequencies.

All illustrations of the optimized geometries were produced by the program Visualization for Electronic and Structural Analysis (VESTA) [43].

3. Results and Discussion

Atomically resolved STM images of the Co(11-20) surface are displayed in Figure 2. The surface is composed of zigzag rows of atoms along the [0001] direction, indicated in the figure along with the (1x1) unit cell (Fig. 2b). The presence of point defects and/or contaminants is observed as small depressions and protrusions together with the regular pattern from the Co atom zigzag rows. The HR-PES measurements showed that minor amounts of carbon species could be present after the cleaning procedure, reflecting the highly reactive nature of Co which makes it difficult to remove all traces of residual contaminants from the surface. Residual carbon on the clean Co surface has previously been encountered in HR-PES investigations of CO dissociation on Co(0001) [44], from which relevant and interesting conclusions could be reached despite the trace contamination.

Figure 3a displays an STM image of step edge(s) on clean Co(11-20). The zigzag rows are well resolved on the terraces and at the monoatomic step. The height of the monoatomic step is ~1.25 Å. The white features marked by circles in the lower right corner of the image are due to contaminants. Upon adsorption of K, the appearance of the Co(11-20) surface as recorded by STM changes. This is shown in the image of Figure 3b, recorded after deposition of a submonolayer coverage of K, for which no ordered overlayer structure could be observed by LEED. In this case, the zigzag rows characteristic of the Co(11-20) surface are resolved

on the terraces, whereas the step edges are no longer well resolved. The step edges have become blurred and displays a number of irregular dark features below the edge with characteristic dimensions larger than the distance between the zigzag rows for the clean surface; up to 10 Å. Norris et al. [45,46] previously found that individual K atoms imaged by STM on the surface of Ni(100)(2×2)p4g-N displayed a larger radius than the reported atomic (2.35 Å) and ionic radius (1.33 Å). This, together with the observed blurriness and irregular features, are possible indications that K is located near or at the step edges. However, the actual site of K, below or on top of the step edges, is difficult to determine from the STM images. K adsorbed on Cu(100) and Cu(110) was observed as depressions when imaged by STM [47], and explained as a result of charge redistribution between K and Cu. Similar charge redistribution from adsorbed K to Co may occur in the present case. The effective radius of K (R_{eff}) for the most favorable adsorption site (t_B, see below) is calculated as 1.96 Å (Table 1), which is considerably smaller than the diameter of the observed irregular features at the step edges. However, difference electron density plots for K adsorbed on Co(10-10) [48] and Co(10-11) and Co(10-12) [49] show that the charge redistribution includes the neighboring Co atoms in the topmost layer. Hence adsorbed K atoms would possibly image as features larger than the effective K radius in STM.

DFT investigations were performed to predict the possible adsorption sites of K on Co(11-20). The energetically favoured geometry on Co(11-20) with one K adsorbed per (3x2) unit cell is illustrated in Figure 4. The stable high symmetry site, corresponding adsorption energy and structural values are listed in Table 1. K favors adsorption in the top site in layer B, labeled t_B in Figure 1, in between the zigzag rows of the outermost surface layer A, with an adsorption energy of -2.02 eV. The same site and similar adsorption energy was calculated by Chen et al [49]. They estimated the highest adsorption energy for (10-12), at -2.40 eV, between all the possible terminations present for the Wulff construction of the equilibrium

194 shape of hcp cobalt [49]. Table 1 also includes calculations for adsorption of 2 K atoms per
195 (3x2) unit cell to investigate the effect of increased coverage. The separation by one zigzag
196 row is more favorable (E_{ads} = -1.92 eV) than two K atoms being located in the same row (E_{ads}
197 = -1.73 eV), suggesting that agglomeration of K on the surface is unlikely. The decrease in
198 adsorption energies for higher K coverage indicates a repulsive interaction between the K
199 atoms, in agreement with previous experimental [25,28] and modeling [49] investigations of
200 Co, as well as other transition metal surfaces [50,51].

201 The appearance of the step edges as recorded by STM upon K deposition (Fig. 3b), combined
202 with favoured adsorption of K atop the Co atoms in layer B, as well as the repulsive
203 interaction between the K atoms, indicate that migration of K along the layer B rows and to
204 the step edges is possible. Assessment of diffusions barriers are required to complete this
205 picture. Calculations were therefore performed applying the NEB method for selected
206 diffusion paths. This yielded a barrier of ~0.02 eV for diffusion along the [0001] direction
207 between the zigzag rows of the outermost surface layer (between atop sites in layer B). The
208 diffusion path across a row, perpendicular to the [0001] direction, resulted in a significantly
209 higher barrier of ~0.2 eV. This supports anisotropic diffusion of K on Co(11-20). A similar
210 result has also been obtained on Co(10-12), while the more close-packed and symmetric
211 terminations generally yield low diffusion barriers [49]. Directionally dependent diffusion of
212 K has also previously been observed experimentally on W(112), with the K-atoms diffusing
213 along [-1-11] channels in the surface [52].

214 The absence of stable adsorption sites in the topmost layer A shows that it is favourable for K
215 to be highly coordinated with Co, further indicating that K is likely to be located at e.g step
216 edges or point defects on the terrace. It was inferred from the STM images in Figure 3 that K
217 may be situated near the step edges. To further address this issue, the adsorption at sites
218 above or below a step edge was simulated by creating a pseudo step within a (3x4) surface

unit cell, as illustrated in Figure 5. The adsorption of K below the pseudo-step resulted in a larger adsorption energy (see Table 2) compared to adsorption further away from the edge. The latter adsorption energy is slightly higher than the t_B value obtained for the (3x2) surface (Table 1) due to coverage effects. The preferred adsorption site beneath the pseudo step is slightly off the t_B site (denoted as offset t_B), with a bond length of 3.35 Å between the adsorbed K atom and the Co atom at the edge. No stable adsorption sites above the pseudo-step edge were obtained. This, together with the low barriers of diffusion for K along the [0001] direction further strenghtens the notion that K migrates relatively easily until encountering an obstacle such as a step edge, where it stabilizes. Point defects, such as those observable on the clean Co(11-20) surface in Figure 2a may also stabilize K. Calculations where a single Co atom has been removed were found to yield a K-stabilizing effect.

The effect of K on the CO induced (3x1)-reconstruction is important to the discussion of the deactivation of Co-based catalysts in FTS, as well as to the nature of the active surface. The CO induced reconstruction of clean Co(11-20) monitored by STM during CO exposure is displayed in Figure 6. At low exposures (1.7 L), troughs start to develop at the step edges. The troughs expand along the [0001] direction with increasing CO exposure. The restructuring proceeds in a highly anisotropic manner; which is particularly apparent for step edges perpendicular to the [0001] direction. These findings are in line with the previously reported surface reconstruction [22,24], involving anisotropic, CO induced transport of Co along the the zigzag rows of the Co(11-20) surface and resulting in (3x1) periodicity in well ordered areas [22]. The latter is also confirmed by LEED at saturation coverage (~4-6 L, not shown). Ridges and troughs developing on the terraces from neighboring step edges eventually meet after which the propagation stops. There is a small amount of contamination at the step edges marked with yellow circles. The presence of these contaminants obstructs formation of troughs or ridges from these locations.

The CO induced restructuring process observed for the Co(11-20) surface with predeposited K differs from the reconstruction upon CO exposure of the clean surface. The images in Figure 7 contains screw dislocations as opposed to the clean surface in Figure 6, but were chosen because of imaging quality. However, the differences observed extend to the entire step edge as well as the terraces and similar development under CO exposure with K preadsorbed has been observed with STM for step edges without screw dislocations. As shown in Figure 7, the formation of troughs on the surface with K mainly initiates on the terraces and not from the step edges. Moreover, restructuring is first observed after about 3.9 L CO, an exposure where the (3x1) reconstruction is close to fully developed on clean Co(11-20). With adsorbed K, the step edges remain to a large degree intact, and ridges growing from the step are not observed as in the case of CO adsorption in absence of K. The results thus infer that the migration of Co from and to the step edges is obstructed by K. The slower initiation and progress of the restructuring also indicates a higher activation barrier. This could be associated with a higher energy associated with removing Co atoms from the terrace or a higher density of diffusing Co species; as a result of the sites near the step edges being unavailable due to the presence of K. Disturbances in STM images, which is increasing through Fig. 7b-e, is often related to interaction between the STM tip and mobile species on the surface [53,54].

Extending the CO exposure to 8.9 L does not result in a fully reconstructed surface, and (3x1) periodicity could not be observed locally by STM (Fig. 7f). The LEED image (not shown) displays a diffuse (3x1)-pattern, hence confirming a lower degree of order for the reconstructed surface. A high amount of small protrusions can be seen, presumably Co that has agglomerated into immobilized islands. This can be attributed to a high density of diffusing species as a result of the sites near the step edge being unavailable. It cannot be

completely excluded that also the presence of some K on the terraces, e.g. adsorbed at point defects, have inhibited the migration of Co and thereby immobilized the agglomerates.

The effect of pre-deposited K on CO adsorption at RT was further investigated with HR-PES. K 2p and C 1s core level spectra for high CO exposure of Co(11-20) have been compared to their unexposed counterparts for two levels of K submonolayer dosing as well as without in Figure 8. The measurement with the smallest amount of K deposited on Co(11-20) is denoted as level 1, and the largest deposition as level 2. The respective amounts of deposited K were estimated to be 0.6% and 2% of the Co surface area. The C 1s spectrum obtained for clean Co(11-20) shows a small peak located at 282.9 eV, which can be attributed to carbidic carbon [55,56]. This peak is present also after K deposition (no CO), with a minor increase with coverage. In addition, a peak at binding energy 284.6 eV can be attributed to graphitic carbon [55,56] for the surface with the highest amount of K. This shows that the deposition of K carries some C, either from the K source or the evaporator. It is important to note that there is no significant increase in these carbon peaks after CO adsorption.

The spectra displayed in Fig. 8 are for very high CO exposures, but similar results were obtained for measurements applying exposures near saturation as indicated from the STM results, i.e. in the order of 5-10 L. Molecular adsorption has previously been found for adsorption of CO on clean Co(11-20) at RT [24]. Our results are in agreement with this observation, and the CO peak is located at binding energy 285.4 eV on the clean surface. Upon considering the relative peak intensities of K 2p and C 1s it is important to note that the cross section for K 2p (2.128 for hv=370 eV) is larger than for C 1s (0.561) [57,58]. The cross section corrected ratio between the CO C 1s and the K $2p_{3/2}$ peak is 2.88 for level 1 and 0.83 for level 2. A smaller amount of CO is nevertheless present on the surfaces with submonolayer amounts of predeposited K as compared to CO adsorption on clean Co(11-20). The ratio between the amount of adsorbed CO on the clean surface and the surfaces with

predeposited K is 0.6±0.1 for both level 1 and 2. There is also a slight shift towards lower binding energy for the CO C 1s core level with K co-adsorbed; ~0.1 eV and ~0.2 eV for lowest and highest K coverage, respectively. Such small shifts indicate that there is no significant change in the CO adsorption site due to the presence of K, and the values are close to previous reports for low coverages of K on polycrystalline Co with adsorbed CO [59]. The K 2p peaks (K $2p_{1/2}$ located at 296.4 eV, and K $2p_{3/2}$ and located at 293.6 eV) did not shift in binding energy upon CO adsorption. The lack of correlation between the amount of CO adsorbed and the level of K predeposited indicates that the reduced CO coverage can not be ascribed to K simply covering the surface. This is in line with the aforementioned significant decrease in activity found for Co-based FTS catalysts with small alkali metal loadings (<1000 ppm) [7,10,11].

The PES results imply that the presence of K does not promote CO dissociation at RT, and that the total amount of CO adsorbed on the surface is reduced, albeit with no significant correlation in the amount adsorbed relative to the amount of predeposited K for the coverages applied. This may be partially in contrast to Vaari et al. [60], who reported that a monolayer of predeposited K on a polycrystalline Co foil resulted in a threefold increase in the CO saturation exposure in comparison to a clean foil. However, our K coverages are significantly lower. Furthermore, the saturation exposure for CO at RT on Co(0001) results in a (√3x√3)R30° CO overlayer structure, corresponding to a coverage of θ=1/3 ML [61,62] and no observable Co migration [61]. Whereas a significant restructuring of the Co takes place on Co(11-20) [22] and Co(10-12) [23], the resulting coverage is not known.

The final investigation within the scope of this work has been the modelling of co-adsorption of potassium and CO by DFT, applying a (3x2) unreconstructed Co(11-20) surface slab (without the pseudo-step). The most favourable sites obtained, with corresponding parameters are shown in Table 3, where the adsorption of CO only is included for comparison. The

preferred adsorption site for CO is b_A, with an adsorption energy of -1.60 eV. For the co-adsorbed system, the most stable configuration is found when CO is located in the vicinity of K, as shown in Figure 9. Furthermore, CO still favours adsorption in the same site (b_A) as for the surface without K present, in agreement with the HR-PES C 1s results discussed above. The adsorption of CO on Co(11-20) with K preadsorbed results in an adsorption energy of -1.93 eV (Table 3). This is higher than without K, and suggests that CO is stabilized by the presence of K. The C-O bond is correspondingly weakened by the interaction with K, with an increase in bond length by 0.03 Å relative to the CO/Co(11-20) system. This can be understood through the increased backdonation from the Co substrate into the CO $2\pi^*$ anti bonding states caused by the charge redistribution from K to Co [63]. The stabilization of CO by K is in line with XPS and TDS measurements on polycrystalline Co [59,60], Co(0001) [27] and Co(10-10) [29], where preadsorbed K resulted in an increased CO desorption temperature. Moreover, increased CO heat of adsorption was obtained on K/Ni(100) by single crystal adsorption microcalorimetry [64]. This stabilization effect of alkali on CO, as well as the bond elongation, has also been obtained by DFT modelling of CO+K coadsorption on Fe(100) [65] and Pd(111) [66]. With respect to FTS, this appears to signify the importance of CO stabilization in dissociating CO and sustain the active carbide phase for Fe [9], while this picture is different for Co.

It may be advocated that the CO+K stabilizing effect impedes the CO-induced restructuring as observed by the slow and disordered development of troughs on the terraces in Figure 7. The predeposited K also appears to be stabilized on sites on the terraces and at the step edges, from which the migration of Co is initiated in the absence of K. However, the blocking of active sites alone is not considered likely to be the cause of the lower amount of CO adsorbed on the surface. The influence of K on the migration process of Co could result in alterations to the amount of CO adsorbed, through the surface configuration being less energetically

favourable for CO adsorption. The obstructed migration process may be due to a combination of several factors; stabilization of CO by K, the removal of Co from as well as its addition to the step edges being hindered by the presence of K, and consequently a higher energy barrier for the removal of Co from terrace sites.

Claiming relevance of these results for Fischer-Tropsch synthesis over supported Co particles should be handled with care, not only given the gap in conditions (P,T), but also considering the relevance of the Co(11-20) termination and the structure sensitivity of the FTS. Previous ex-situ Electron Energy Loss Spectroscopy (EELS) and Auger Electron Spectroscopy (AES) investigations of Co(0001), Co(10-12) and Co(11-20) single crystals exposed to Fischer Tropsch reaction conditions (1 bar, H_2:CO=2, T=493-543 K) showed significant differences in the chain growth probabilities of the three surfaces [67]. It has also been debated to which extent the particles undergo an hcp-to-fcc transition under reaction conditions, and in any case the (11-20) facet is not predicted to dominate the hcp particle Wullf construction [49]. But as mentioned initially, several investigations point to the possibility of the Co particles restructuring [14,18,19]. Our results therefore suggest that predeposited, submonolayer amounts of K leads to overall higher energy barriers for any restructuring associated with mobility of Co atoms along the surface of the particles, and that such restructuring is important to the high activity during synthesis.

4. Conclusions

The depositon of submonolayer amounts of K on the surface of Co(11-20) and the subsequent effect on the adsorption of CO was investigated with STM, HR-PES and DFT. The calculations predicted that adsorption of K was favoured in sites between the zigzag-rows of the topmost layer, with associated low barriers of diffusion along the [0001] direction. The

appearance of the step edges as imaged by STM after deposition of K,, together with the DFT calculations, suggested that K was situated near the step edges for low coverages. The restructuring of the surface as monitored with STM, involving the migration of Co atoms, proceeded at the terraces rather than the step edges with K pre-deposited. The migration of Co appeared obstructed, resulting in a slower and more disordered restructuring, which may indicate a higher activation energy for the process. In agreement with previous studies of co-adsorption of alkali and CO on transition metal surfaces, the calculations indicate a stabilizing effect on CO from predeposited K. On the other hand, HR-PES showed that the amount of CO adsorbed on the surface decreased significantly with predeposited K, . but no further change in the amount of CO adsorbed was found upon increasing amount of predeposited K. We thus attribute the reduced amount of CO adsorbed on the surface to the small amounts of K obstructing the restructuring of the Co(11-20) surface.

5. Acknowledgments

Financial support has been received from inGAP (Innovative Natural Gas Processes and Products), a centre for research based innovation appointed by the Research Council of Norway (Project No. 174893/O30), Statoil ASA through the Gas Technology Centre (NTNU-SINTEF) and NTNU. The computations were performed on resources provided by UNINETT Sigma2 - the National Infrastructure for High Performance Computing and Data Storage in Norway, account no. NN9152k and NN9355k, and local resources on Vilje, account no. ntnu946. We thank the ASTRID2 staff for excellent support.

6. References

[1] P.K. Agrawal, J.R. Katzer, W.H. Manogue, Methanation over transition metal catalysts: III. CoAl2O3 in sulfur-poisoning studies, J. Catal. 69 (1981) 327–344. doi:10.1016/0021-9517(81)90169-X.

[2] C.H. Bartholomew, Mechanisms of catalyst deactivation, Appl. Catal. A Gen. 212 (2001) 17–60. doi:10.1016/S0926-860X(00)00843-7.

[3] N.E. Tsakoumis, M. Rønning, Ø. Borg, E. Rytter, A. Holmen, Deactivation of cobalt based Fischer–Tropsch catalysts: A review, Catal. Today. 154 (2010) 162–182. doi:10.1016/j.cattod.2010.02.077.

[4] M.E. Dry, The Fischer–Tropsch process: 1950–2000, Catal. Today. 71 (2002) 227–241. doi:10.1016/s0920-5861(01)00453-9.

[5] S. Arvelakis, E.G. Koukios, Physicochemical upgrading of agroresidues as feedstocks for energy production via thermochemical conversion methods, Biomass and Bioenergy. 22 (2002) 331–348. doi:http://dx.doi.org/10.1016/S0961-9534(01)00056-3.

[6] R.L. Espinoza, A.P. Steynberg, B. Jager, A.C. Vosloo, Low temperature Fischer–Tropsch synthesis from a Sasol perspective, Appl. Catal. A Gen. 186 (1999) 13–26. doi:10.1016/s0926-860x(99)00161-1.

[7] C. Balonek, A. Lillebø, S. Rane, E. Rytter, L. Schmidt, A. Holmen, Effect of Alkali Metal Impurities on Co–Re Catalysts for Fischer–Tropsch Synthesis from Biomass-Derived Syngas, Catal. Letters. 138 (2010) 8–13. doi:10.1007/s10562-010-0366-4.

[8] Ø. Borg, N. Hammer, B.C. Enger, R. Myrstad, O.A. Lindvåg, S. Eri, T.H. Skagseth, E. Rytter, Effect of biomass-derived synthesis gas impurity elements on cobalt Fischer–Tropsch catalyst performance including in situ sulphur and nitrogen addition, J. Catal. 279 (2011) 163–173. doi:10.1016/j.jcat.2011.01.015.

[9] H. Schulz, Selforganization in Fischer–Tropsch synthesis with iron- and cobalt catalysts, Catal. Today. 228 (2014) 113–122. doi:http://dx.doi.org/10.1016/j.cattod.2013.11.060.

[10] A.H. Lillebø, E. Patanou, J. Yang, E.A. Blekkan, A. Holmen, The effect of alkali and alkaline earth elements on cobalt based Fischer–Tropsch catalysts, Catal. Today. 215 (2013) 60–66. doi:10.1016/j.cattod.2013.03.030.

[11] E. Patanou, A.H. Lillebø, J. Yang, D. Chen, A. Holmen, E.A. Blekkan, Microcalorimetric Studies on Co–Re/γ-Al 2 O 3 Catalysts with Na Impurities for Fischer–Tropsch Synthesis, Ind. Eng. Chem. Res. 53 (2014) 1787–1793. doi:10.1021/ie402465z.

[12] P.L. Hansen, J.B. Wagner, S. Helveg, J.R. Rostrup-Nielsen, E. Al, Atom-resolved imaging of dynamic shape changes in supported copper nanocrystals, Science (80-.). 295 (2002) 2053–2055. http://search.proquest.com/docview/213582162?accountid=12870.

[13] S.B. Vendelbo, C.F. Elkjær, H. Falsig, I. Puspitasari, P. Dona, L. Mele, B. Morana, B.J. Nelissen, R. van Rijn, J.F. Creemer, P.J. Kooyman, S. Helveg, Visualization of oscillatory behaviour of Pt nanoparticles catalysing CO oxidation, Nat. Mater. 13 (2014) 884–890. doi:10.1038/nmat4033.

[14] J. Wilson, C. de Groot, Atomic-Scale Restructuring in High-Pressure Catalysis, J.

436 Phys. Chem. 99 (1995) 7860–7866. doi:10.1021/j100020a005.
437 [15] H. Schulz, Z. Nie, F. Ousmanov, Construction of the Fischer–Tropsch regime with
438 cobalt catalysts, Catal. Today. 71 (2002) 351–360.
439 doi:http://dx.doi.org/10.1016/S0920-5861(01)00462-X.
440 [16] C.J. Weststrate, A.C. Kızılkaya, E.T.R. Rossen, M.W.G.M. Verhoeven, I.M. Ciobîcă,
441 A.M. Saib, J.W. (Hans) Niemantsverdriet, Atomic and Polymeric Carbon on
442 Co(0001): Surface Reconstruction, Graphene Formation, and Catalyst Poisoning, J.
443 Phys. Chem. C. 116 (2012) 11575–11583. doi:10.1021/jp301706q.
444 [17] M. Ehrensperger, J. Wintterlin, In situ high-pressure high-temperature scanning
445 tunneling microscopy of a Co(0001) Fischer–Tropsch model catalyst, J. Catal. 319
446 (2014) 274–282. doi:http://dx.doi.org/10.1016/j.jcat.2014.09.011.
447 [18] K. Høydalsvik, J.B. Fløystad, A. Voronov, G.J.B. Voss, M. Esmaeili, J. Kehres, H.
448 Granlund, U. Vainio, J.W. Andreasen, M. Rønning, D.W. Breiby, Morphology
449 Changes of Co Catalyst Nanoparticles at the Onset of Fischer–Tropsch Synthesis, J.
450 Phys. Chem. C. 118 (2014) 2399–2407. doi:10.1021/jp4052193.
451 [19] A. Banerjee, V. Navarro, J.W.M. Frenken, A.P. van Bavel, H.P.C.E. Kuipers, M.
452 Saeys, Shape and Size of Cobalt Nanoislands Formed Spontaneously on Cobalt
453 Terraces during Fischer–Tropsch Synthesis, J. Phys. Chem. Lett. 7 (2016) 1996–2001.
454 doi:10.1021/acs.jpclett.6b00555.
455 [20] A. Banerjee, A.P. van Bavel, H.P.C.E. Kuipers, M. Saeys, Origin of the Formation of
456 Nanoislands on Cobalt Catalysts during Fischer–Tropsch Synthesis, ACS Catal. 5
457 (2015) 4756–4760. doi:10.1021/acscatal.5b01169.
458 [21] M. Ehrensperger, J. Wintterlin, In situ scanning tunneling microscopy of the poisoning
459 of a Co(0001) Fischer–Tropsch model catalyst by sulfur, J. Catal. 329 (2015) 49–56.
460 doi:10.1016/j.jcat.2015.04.028.
461 [22] H.J. Venvik, A. Borg, C. Berg, Formation of the CO-induced (3 × 1) surface structure
462 on Co(11-20) studied by STM, Surf. Sci. 397 (1998) 322–332. doi:10.1016/s0039-
463 6028(97)00751-6.
464 [23] H.J. Venvik, C. Berg, A. Borg, CO adsorption on Co(10$\bar{1}$2) – a STM study, Surf. Sci.
465 402–404 (1998) 57–61. doi:10.1016/s0039-6028(97)01023-6.
466 [24] H. Papp, Chemisorption and reactivity of carbon monoxide on a Co(11$\bar{2}$0) single
467 crystal surface; Studied by LEED, UPS, EELS, AES and work function measurements,
468 Surf. Sci. 149 (1985) 460–470. doi:http://dx.doi.org/10.1016/0039-6028(85)90075-5.
469 [25] T. Vaara, J. Vaari, J. Lahtinen, Adsorption of Potassium on Co(0001), Surf. Sci. 395
470 (1998) 88–97. doi:10.1016/S0039-6028(97)00618-3.
471 [26] J. Vaari, J. Lahtinen, P. Hautojärvi, The adsorption and decomposition of acetylene on
472 clean and K-covered Co(0001), Catal. Letters. 44 (1997) 43–49.
473 doi:10.1023/a:1018972924563.
474 [27] J. Vaari, J. Lahtinen, T. Vaara, P. Hautojärvi, An XPD and ISS study of the (2 × 2)-
475 (CO + K) coadsorption structure on Co(0001), Surf. Sci. 346 (1996) 1–10.
476 doi:10.1016/0039-6028(95)00917-5.
477 [28] J. Lahtinen, J. Vaari, T. Vaara, K. Kauraala, P. Kaukasoina, M. Lindroos, LEED
478 investigations on Co(0001): the clean surface and the (2×2)-K overlayer, Surf. Sci. 425
479 (1999) 90–100. doi:10.1016/S0039-6028(99)00188-0.
480 [29] R.L. Toomes, D.A. King, The coadsorption of CO and K on Co{100}, Surf. Sci. 349

(1996) 19–42. doi:10.1016/0039-6028(95)01050-5.

[30] P. Kaukasoina, M. Lindroos, P. Hu, D.A. King, C.J. Barnes, Full structure determination of an alkali-metal/CO coadsorption phase for Co{101¯0}-c(2×2)-(K+CO), Phys. Rev. B. 51 (1995) 17063–17067. http://link.aps.org/doi/10.1103/PhysRevB.51.17063.

[31] R.L. Toomes, D.A. King, Coadsorption and surface compound formation in the interaction of CO2 with K on Co{1010}, Surf. Sci. 349 (1996) 65–80. doi:10.1016/0039-6028(95)01052-1.

[32] D. Nečas, P. Klapetek, Gwyddion: an open-source software for SPM data analysis, Cent. Eur. J. Phys. 10 (2012) 181–188. doi:10.2478/s11534-011-0096-2.

[33] D.A. Shirley, High-Resolution X-Ray Photoemission Spectrum of the Valence Bands of Gold, Phys. Rev. B. 5 (1972) 4709–4714. doi:10.1103/PhysRevB.5.4709.

[34] S. Doniach, M. Sunjic, Many-electron singularity in X-ray photoemission and X-ray line spectra from metals, J. Phys. C Solid State Phys. 3 (1970) 285–291. doi:10.1088/0022-3719/3/2/010.

[35] G. Kresse, J. Hafner, Ab initio molecular dynamics for liquid metals, Phys. Rev. B. 47 (1993) 558–561. http://link.aps.org/doi/10.1103/PhysRevB.47.558.

[36] J.P. Perdew, K. Burke, M. Ernzerhof, Generalized Gradient Approximation Made Simple, Phys. Rev. Lett. 77 (1996) 3865–3868. http://link.aps.org/doi/10.1103/PhysRevLett.77.3865.

[37] P.E. Blöchl, Projector augmented-wave method, Phys. Rev. B. 50 (1994) 17953–17979. http://link.aps.org/doi/10.1103/PhysRevB.50.17953.

[38] G. Kresse, D. Joubert, From ultrasoft pseudopotentials to the projector augmented-wave method, Phys. Rev. B. 59 (1999) 1758–1775. http://link.aps.org/doi/10.1103/PhysRevB.59.1758.

[39] A. Taylor, R.W. Floyd, No Title, Acta Crystallogr. 3 (1950) 285–289.

[40] H.J. Monkhorst, J.D. Pack, Special points for Brillouin-zone integrations, Phys. Rev. B. 13 (1976) 5188–5192. http://link.aps.org/doi/10.1103/PhysRevB.13.5188.

[41] J.D. Pack, H.J. Monkhorst, “Special points for Brillouin-zone integrations”\char22{}a reply, Phys. Rev. B. 16 (1977) 1748–1749. http://link.aps.org/doi/10.1103/PhysRevB.16.1748.

[42] D. Sheppard, P. Xiao, W. Chemelewski, D.D. Johnson, G. Henkelman, A generalized solid-state nudged elastic band method, J. Chem. Phys. 136 (2012).

[43] K. Momma, F. Izumi, VESTA 3 for three-dimensional visualization of crystal, volumetric and morphology data, J. Appl. Crystallogr. 44 (2011) 1272–1276. doi:10.1107/S0021889811038970.

[44] C.J. Weststrate, P. van Helden, J. van de Loosdrecht, J.W. Niemantsverdriet, Elementary steps in Fischer–Tropsch synthesis: CO bond scission, CO oxidation and surface carbiding on Co(0001), Surf. Sci. 648 (2016) 60–66. doi:10.1016/j.susc.2015.10.050.

[45] A.G. Norris, M.J. Scantlebury, A.W. Munz, T. Bertrams, E. Dudzik, P. Finetti, P.W. Murray, R. McGrath, An STM study of the potassium-induced removal of the Ni(100)(2×2)p4g-N reconstruction, Surf. Sci. 424 (1999) 74–81. doi:10.1016/S0039-6028(99)00014-X.

[46] A.G. Norris, R. McGrath, Coadsorption of potassium at step edges on the Ni(100)(2 × 2)p4g-N reconstructed surface, J. Phys. Condens. Matter. 11 (1999) 9549–9554. doi:10.1088/0953-8984/11/48/312.

[47] G. Doyen, D. Drakova, J. V Barth, R. Schuster, T. Gritsch, R.J. Behm, G. Ertl, Scanning-tunneling-microscope imaging of clean and alkali-metal-covered Cu(110) and Au(110) surfaces, Phys. Rev. B. 48 (1993) 1738–1749. http://link.aps.org/doi/10.1103/PhysRevB.48.1738.

[48] S.J. Jenkins, D.A. King, Adsorbate/substrate bonding in Co{100}/K-c(2×2) elucidated through first-principles theory, Chem. Phys. Lett. 317 (2000) 372–380. doi:10.1016/S0009-2614(99)01336-6.

[49] Q. Chen, I.-H. Svenum, Y. Qi, L. Gavrilovic, D. Chen, A. Holmen, E.A. Blekkan, E. Rytter, U.M. Graham, G.A. Thomas, B.H. Davis, Potassium adsorption behavior on hcp cobalt as model systems for the Fischer–Tropsch synthesis: a density functional theory study, Phys. Chem. Chem. Phys. 19 (2017) 12246–12254. doi:10.1039/C7CP00620A.

[50] E.D. Westre, D.E. Brown, J. Kutzner, S.M. George, Surface diffusion of potassium on Ru(001), Surf. Sci. 294 (1993) 185–196. doi:http://dx.doi.org/10.1016/0039-6028(93)90107-U.

[51] R.D. Diehl, R. McGrath, Structural studies of alkali metal adsorption and coadsorption on metal surfaces, Surf. Sci. Rep. 23 (1996) 43–171. doi:http://dx.doi.org/10.1016/0167-5729(95)00010-0.

[52] B. Bayat, H.-W. Wassmuth, Directional dependence of the surface diffusion of potassium on tungsten (112), Surf. Sci. 133 (1983) 1–8. doi:http://dx.doi.org/10.1016/0039-6028(83)90478-8.

[53] F. Mugele, A. Rettenberger, J. Boneberg, P. Leiderer, Step roughness on Ag(111) investigated by STM: a systematic study of tip influence, Surf. Sci. 377 (1997) 62–65. doi:10.1016/S0039-6028(96)01352-0.

[54] F. Mugele, A. Rettenberger, J. Boneberg, P. Leiderer, The influence of tip–sample interaction on step fluctuations on Ag(111), Surf. Sci. 400 (1998) 80–86. doi:10.1016/S0039-6028(97)00843-1.

[55] J. Nakamura, I. Toyoshima, K. Tanaka, Formation of carbidic and graphite carbon from CO on polycrystalline cobalt, Surf. Sci. 201 (1988) 185–194. doi:http://dx.doi.org/10.1016/0039-6028(88)90605-X.

[56] T. Ramsvik, A. Borg, H.J. Venvik, F. Hansteen, M. Kildemo, T. Worren, Acetylene chemisorption and decomposition on the Co(11-20) single crystal surface, Surf. Sci. 499 (2002) 183–192. doi:10.1016/s0039-6028(01)01795-2.

[57] J.J. Yeh, I. Lindau, Atomic subshell photoionization cross sections and asymmetry parameters: $1 \leqslant Z \leqslant 103$, At. Data Nucl. Data Tables. 32 (1985) 1–155. doi:10.1016/0092-640X(85)90016-6.

[58] WebCrossSections, (n.d.). https://vuo.elettra.eu/services/elements/WebElements.html (accessed May 16, 2017).

[59] D.A. Wesner, G. Linden, H.P. Bonzel, Alkali promotion on cobalt: Surface analysis of the effects of potassium on carbon monoxide adsorption and Fischer-Tropsch reaction, Appl. Surf. Sci. 26 (1986) 335–356. doi:10.1016/0169-4332(86)90074-7.

[60] J. Vaari, J. Lahtinen, P. Hautojärvi, Reactive and thermal properties of CO on

potassium-covered polycrystalline cobalt, Appl. Surf. Sci. 78 (1994) 255–267. doi:http://dx.doi.org/10.1016/0169-4332(94)90013-2.

[61] H.J. Venvik, Adsorbates on cobalt and platinum single crystal surfaces studied by STM, Norwegian University of Science and Technology (NTNU), 1998.

[62] J. Lahtinen, J. Vaari, K. Kauraala, E.A. Soares, M.A. Van Hove, LEED investigations on Co(0001): the (3×3)R30°-CO overlayer, Surf. Sci. 448 (2000) 269–278. doi:10.1016/S0039-6028(99)01228-5.

[63] G. Blyholder, Molecular Orbital View of Chemisorbed Carbon Monoxide, J. Phys. Chem. 68 (1964) 2772–2777. doi:10.1021/j100792a006.

[64] N. Al-Sarraf, J.T. Stuckless, D.A. King, Direct measurement of potassium-promoted change in heat of adsorption of CO on Ni{100}, Nature. 360 (1992) 243–245. http://dx.doi.org/10.1038/360243a0.

[65] D.C. Sorescu, Adsorption and activation of CO coadsorbed with K on Fe(100) surface: A plane-wave DFT study, Surf. Sci. 605 (2011) 401–414. doi:10.1016/j.susc.2010.11.009.

[66] L.-Y. Gan, R.-Y. Tian, X.-B. Yang, Y.-J. Zhao, Theoretical study of the influence of Na on CO adsorption and dissociation on Pd(111): Long-range or short-range interactions between co-adsorbates?, Chem. Phys. Lett. 511 (2011) 33–38. doi:10.1016/j.cplett.2011.06.002.

[67] J.J.C. Geerlings, M.C. Zonnevylle, C.P.M. de Groot, Structure sensitivity of the Fischer-Tropsch reaction on cobalt single crystals, Surf. Sci. 241 (1991) 315–324. doi:10.1016/0039-6028(91)90091-6.

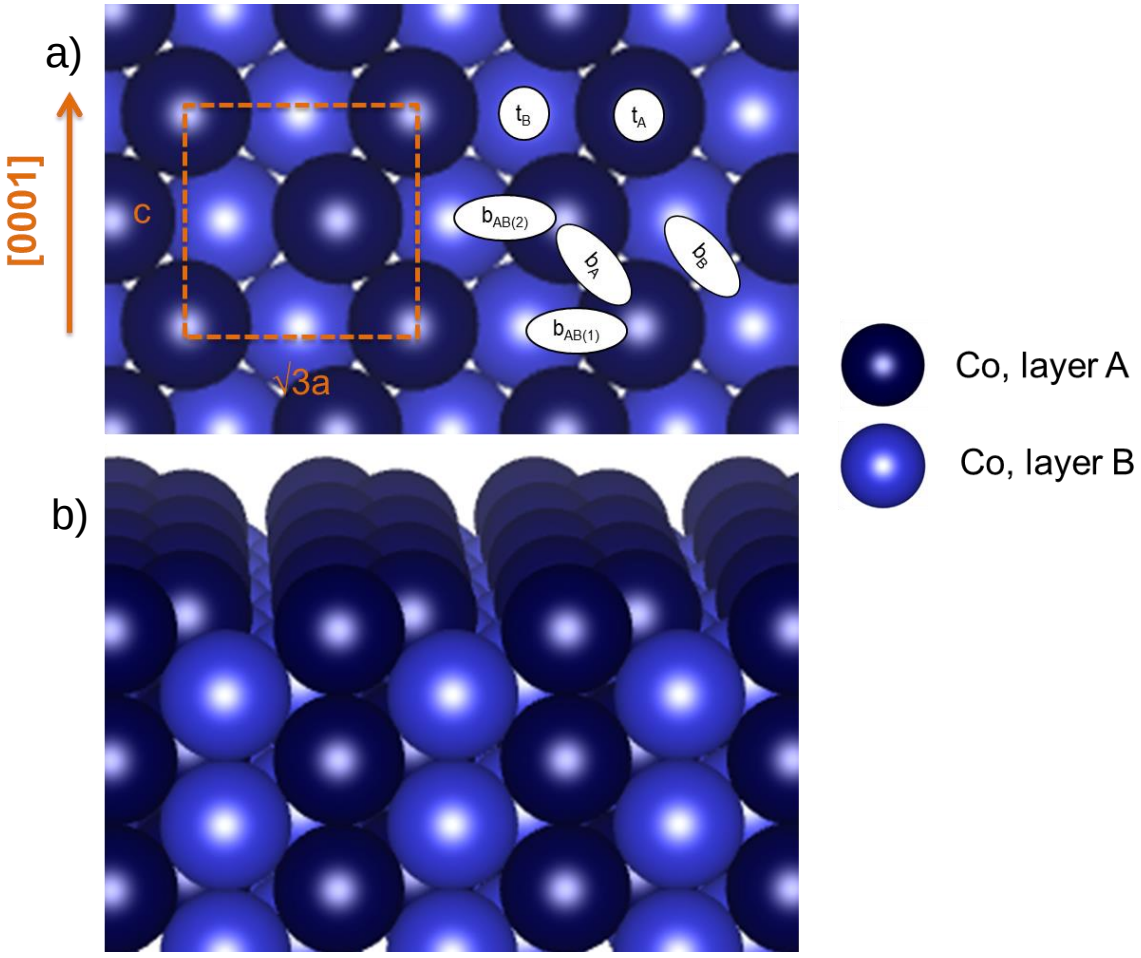

Figure 1: (a) Top and (b) tilted side view illustrations of the Co(11-20) surface model. The (1x1) surface unit cell and the [0001] direction are indicated. The Co atoms are dark blue for the A layer and light blue for the B layer of the hcp stacking. High symmetry sites have been marked as follows: t_A - top position layer A, t_B - top position layer B, b_A - bridge position layer A, b_B bridge position layer B, $b_{AB(1)}$/$b_{AB(2)}$ - bridge position between layer A and B with (1) and (2) denoting two different coordinations.

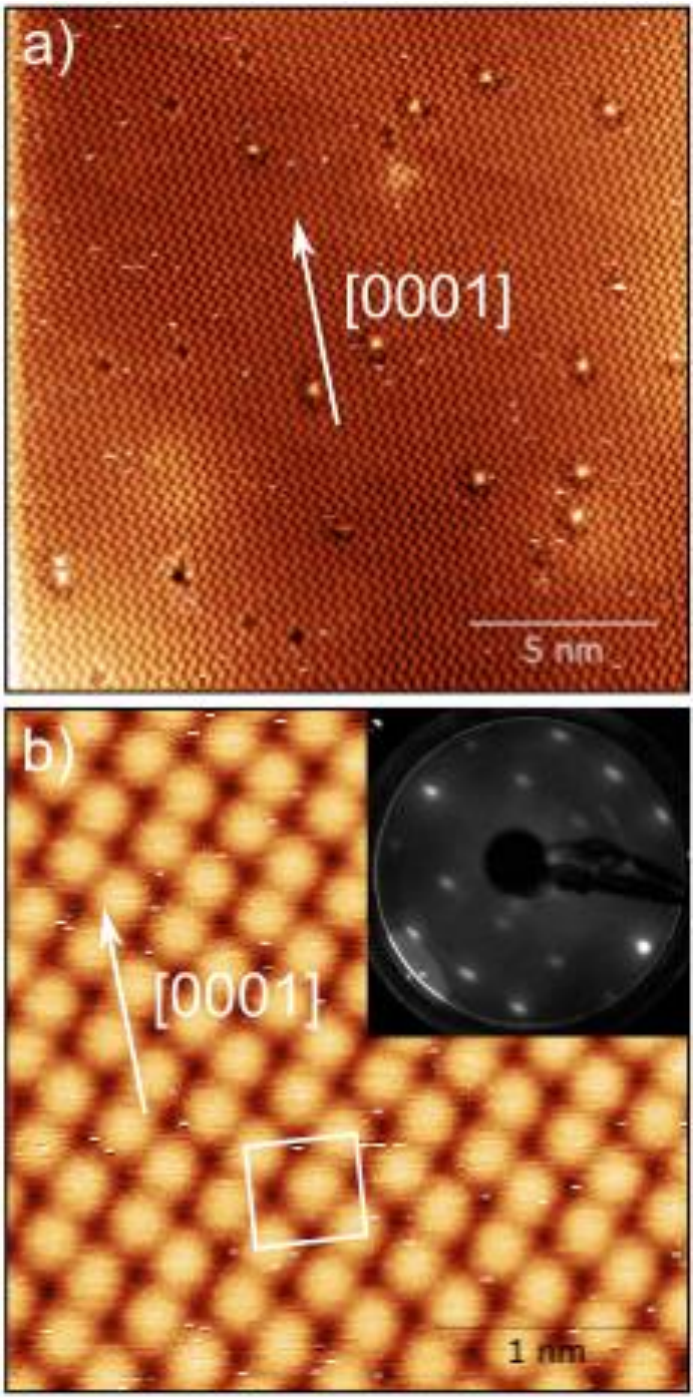

Figure 2: (a) Atomically resolved STM image of the clean Co(11-20) surface showing the [0001]-directed zigzag rows. Some depressions and protrusions due to minor impurities or defects are visible. (b) Affine drift corrected image displaying the individual atoms of the zigzag rows. The (1x1) unit cell is indicated, and the corresponding LEED pattern is displayed in the upper right corner. The images were acquired with bias voltage +0.020 V, and tunneling current 0.70 nA.

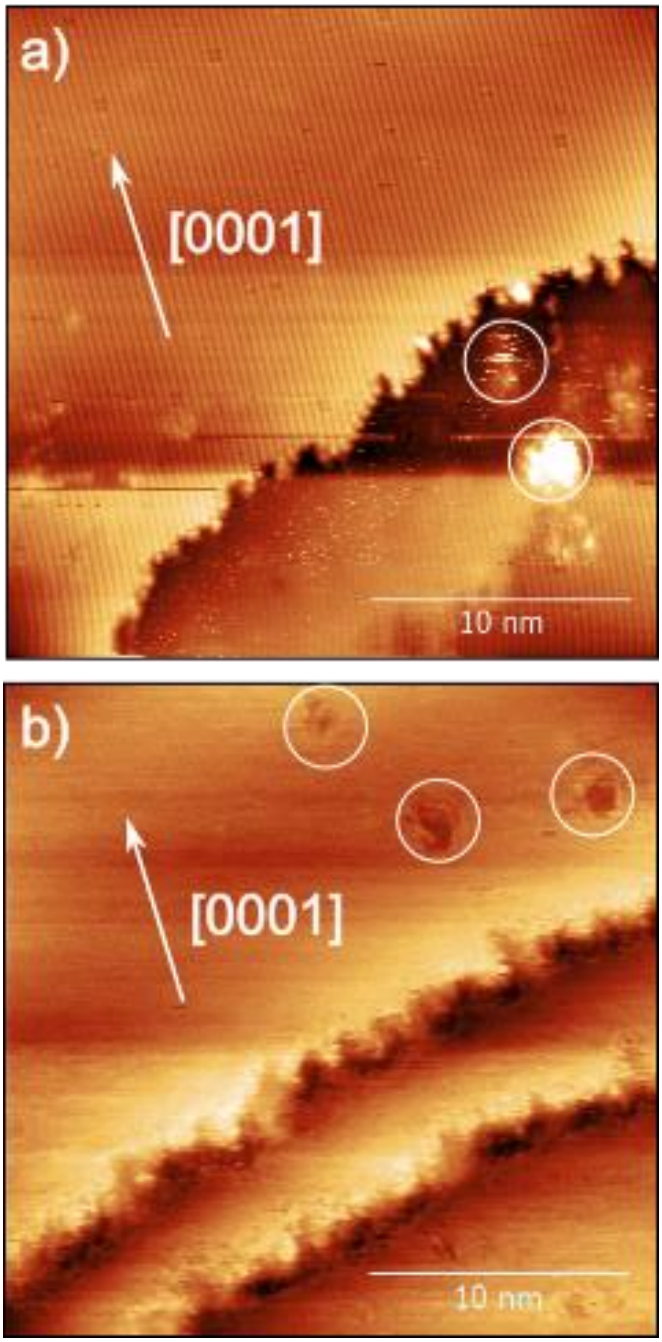

Figure 3: STM images of area 250x250 $Å^2$ of the Co(11-20) surface. (a) Clean surface with monoatomic step, showing the zigzag rows along the [0001] direction, acquired with bias voltage +0.020 V and tunneling current 0.70 nA. (b) The surface with two step edges and submonolayer amounts of K deposited, acquired with bias voltage +0.020 V and tunneling current 5.93 nA. The zigzag rows are visible on the terraces. Contaminants are marked with white circles.

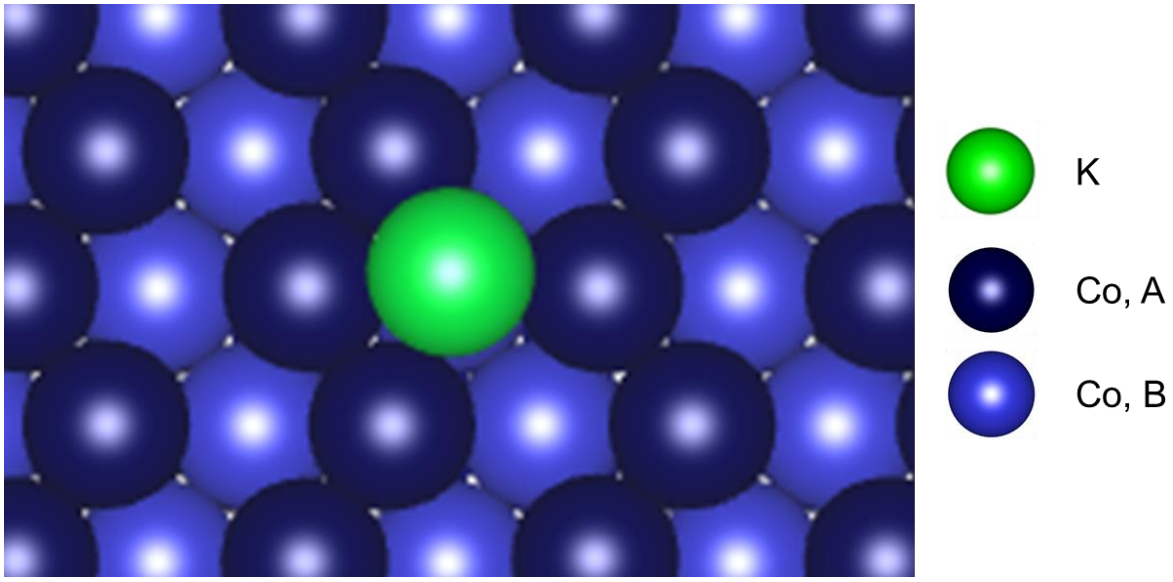

Figure 4: Illustration of the favored adsorption site (t_B) for K on Co(11-20), calculated using one K atom per (3x2) surface unit cell (θ_K=1/24 ML).

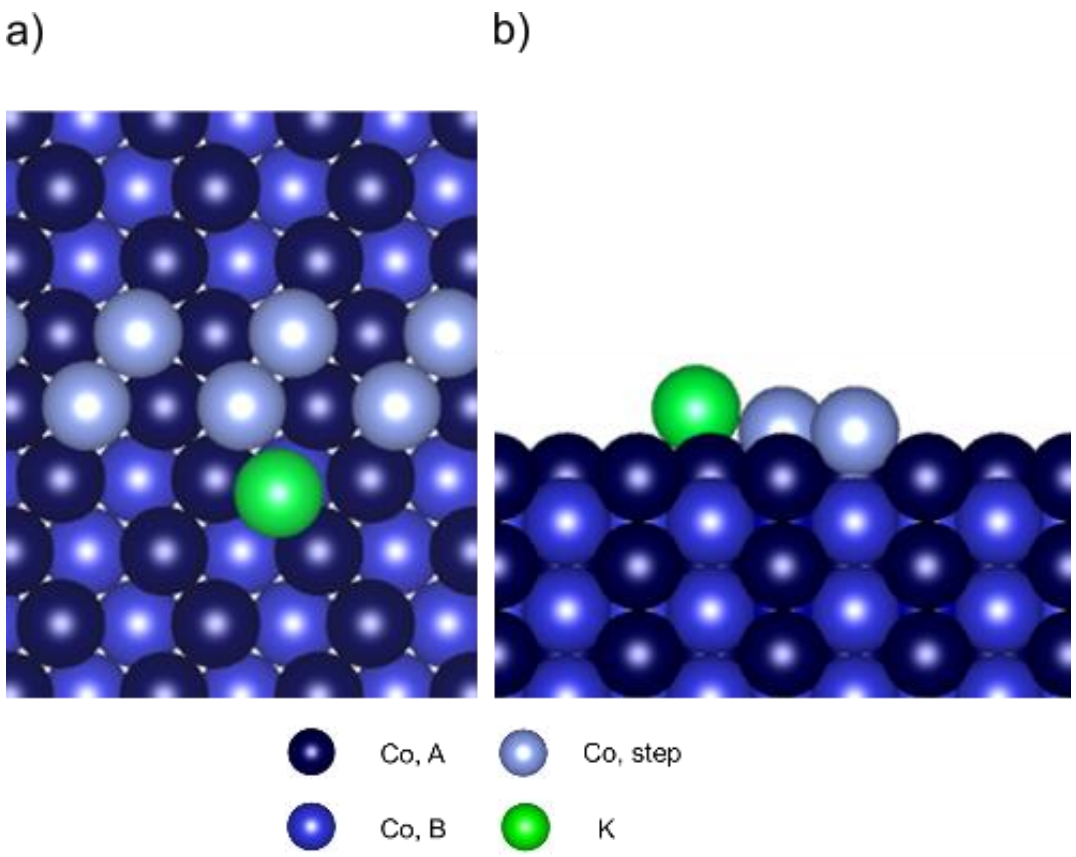

Figure 5: (a) Top and (b) side view of the Co(11-20) surface model with one pseudo step within the (3x4) surface unit cell. K is situated in the favored adsorption site, offset t_B, beneath the pseudo step as predicted from the DFT calculations.

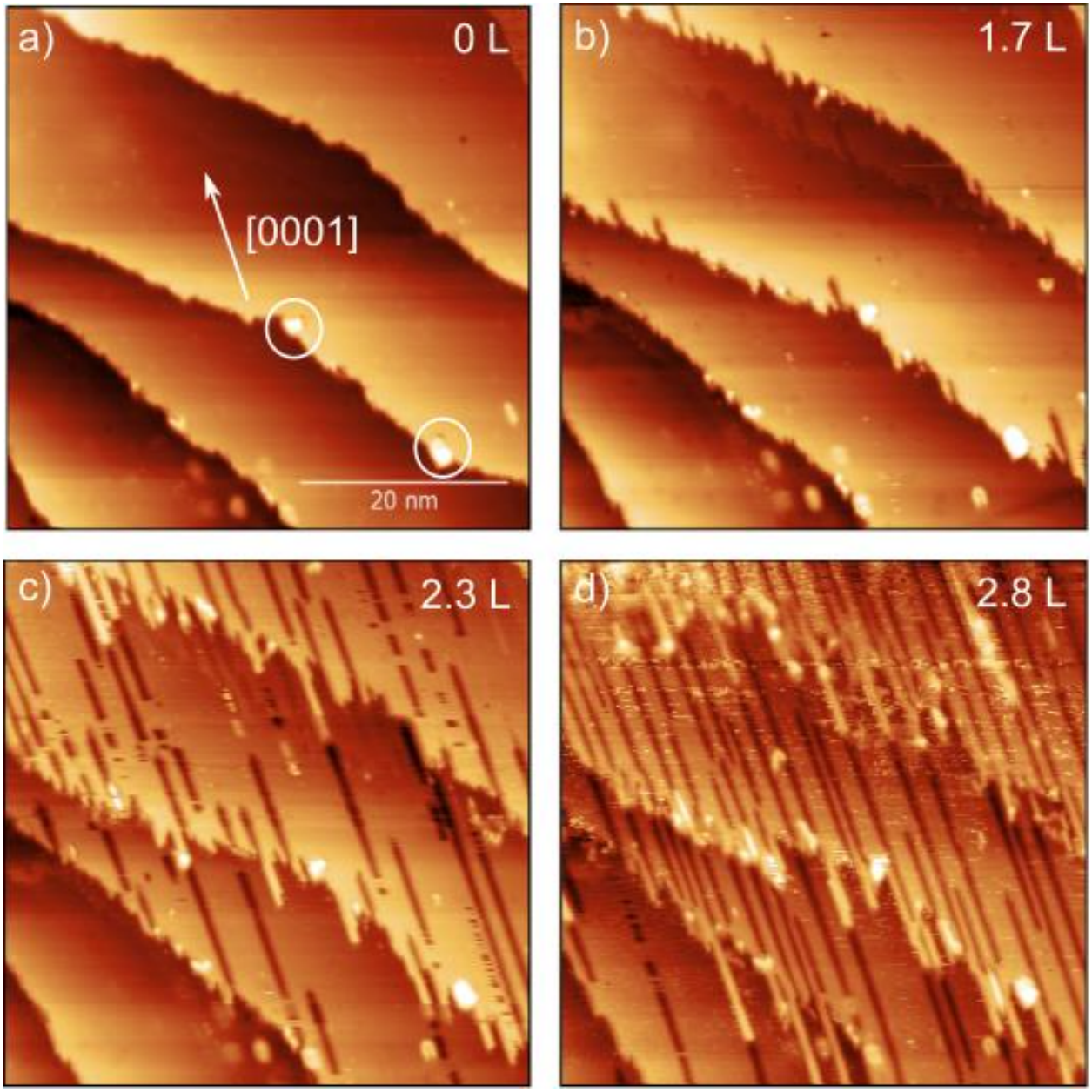

Figure 6: STM images acquired at RT of area 500x500 $Å^2$ of (a) clean Co(11-20) with monoatomic steps and (b)-(d) the same area with increasing CO exposure at $p_{CO} = 2x10^{-9}$mbar; exposure indicated in Langmuir (L). The white circles highlight selected contaminants on the surface. The images were acquired with bias voltage +0.447 V and tunneling current 0.95 nA.

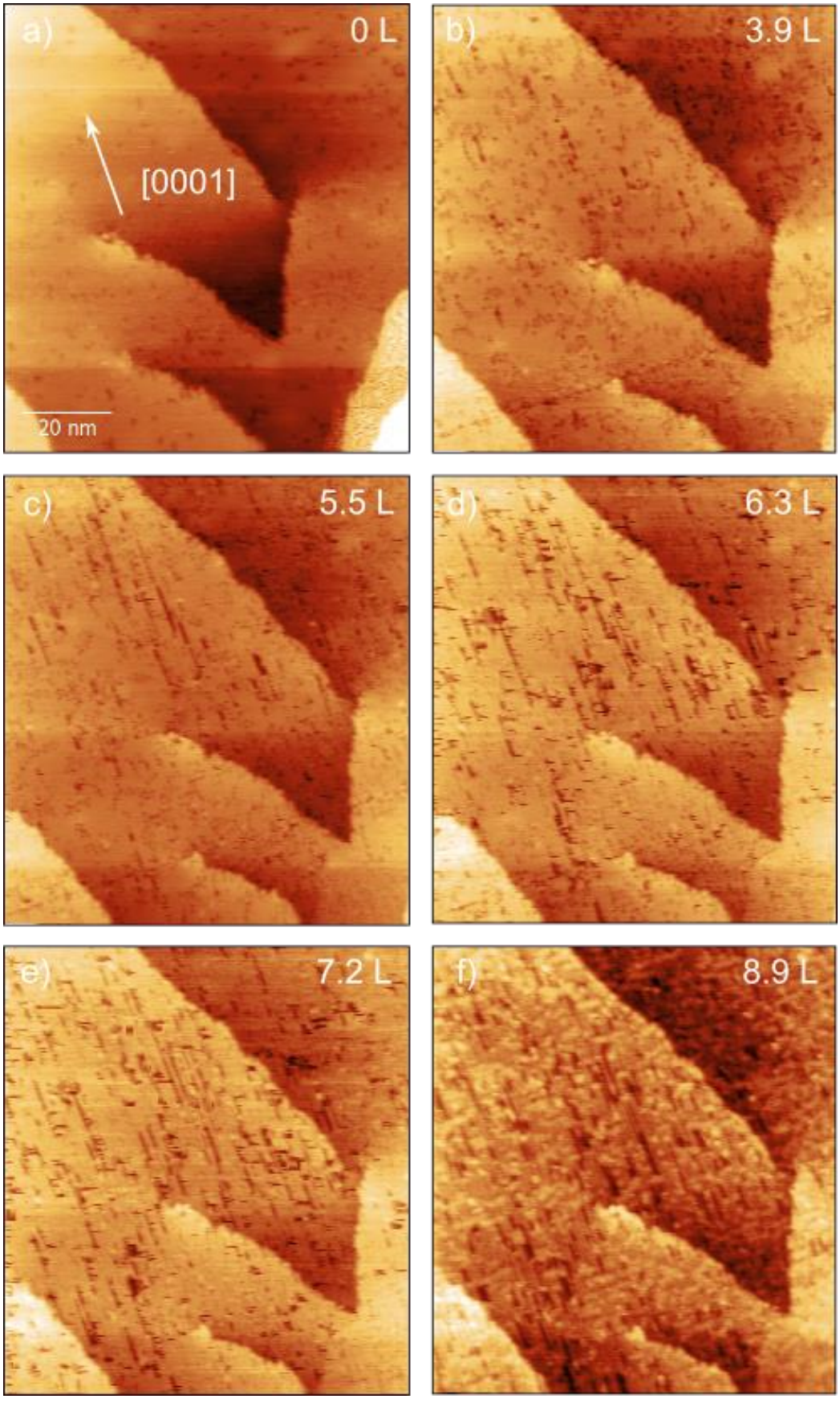

Figure 7: STM images of the surface structure of a 1000x900 $Å^2$ area of Co(11-20) with submonolayer amounts of K, encompassing monoatomic steps, as a function of increasing CO exposure. The images were acquired at RT, during CO exposure at $p_{CO} = 2x10^{-9}$mbar. The exposure of CO in Langmuir (L) is indicated in the upper right corner in images (a)-(f). The images were acquired with bias voltage +0.020 V and tunneling current 0.91 nA.

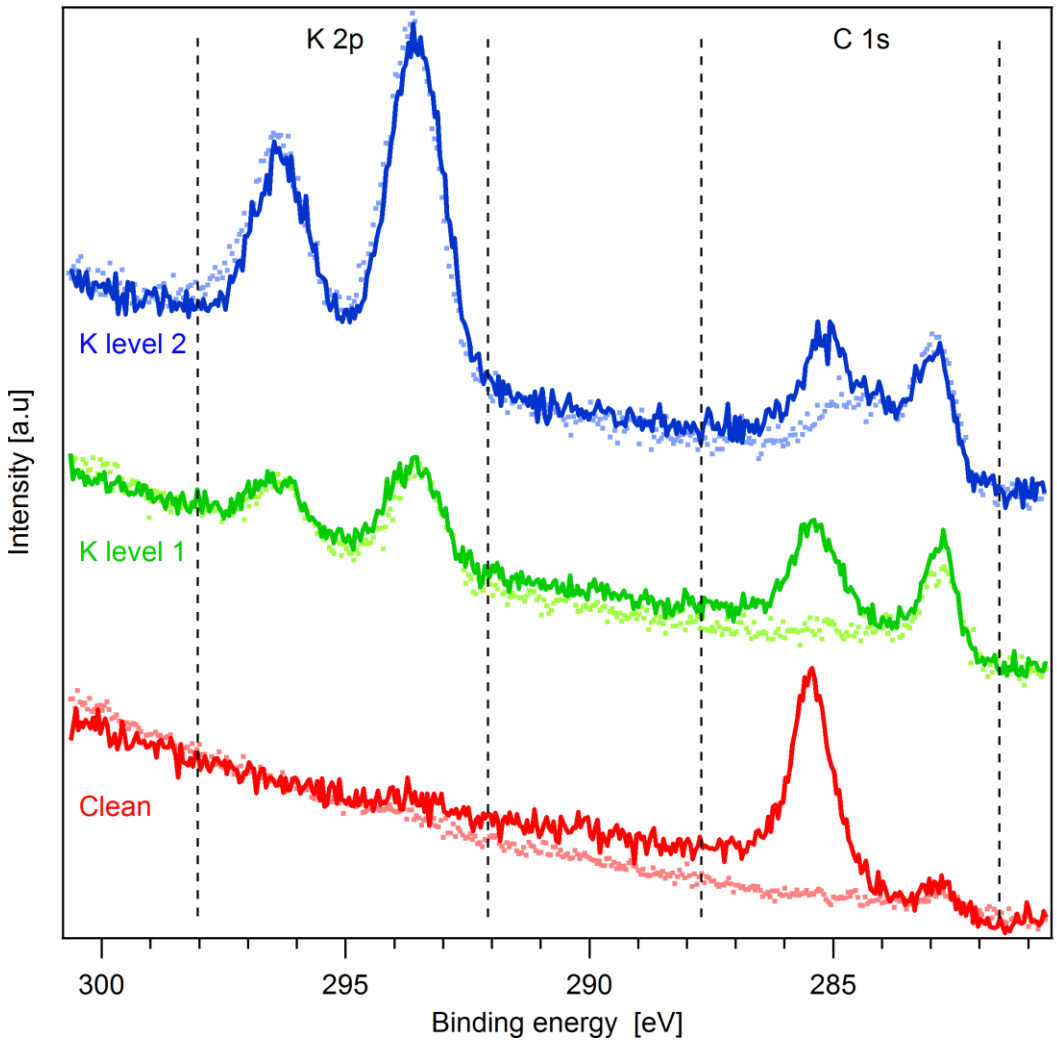

Figure 8: HR-PES of the K 2p and C 1s core levels of the Co(11-20) surface, clean and with K deposited at 2 different submonolayer levels (1 and 2), before and after exposure to CO (85 L). The spectra before exposure is denoted with dotted lines, and the spectra after denoted with a continuous line. Spectra obtained before and after exposure to CO are grouped together: (red) clean Co(11-20), (green) Co(11-20) with K deposited at level 1, (blue) Co(11-20) with K deposited at level 2. All spectra were recorded at RT and a photon energy of 370 eV.

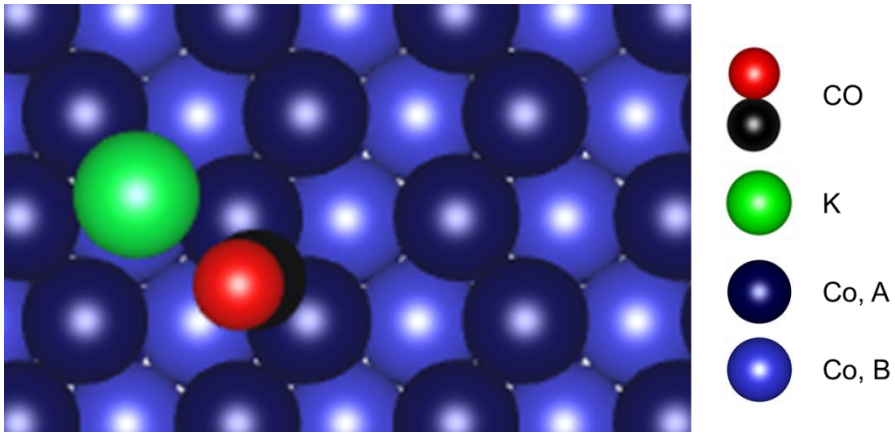

Figure 9: Top view of the preferred adsorption sites of K and CO co-adsorbed on Co(11-20) within the (3x2) surface unit cell (θ_{K+CO} = 1/12 ML). CO is situated in the b_A site and K above layer B as predicted from the DFT calculations.

Table 1: Calculated adsorption energies for K, ($E_{ads,K}$), adsorbed on Co(11-20) within a (3x2) surface unit cell, distance between K and nearest neighbor Co atom (d_{K-Co}), and the effective K radius (R_{eff}).

# K atoms	Adsorption geometry	$E_{ads,K}$ (eV)	d_{K-Co} (Å)	R_{eff} (Å)	Coverage
1	t_B	-2.02	3.20	1.96	θ_K=1/24 ML
2	t_B, separate rows	-1.92	3.14	1.90	θ_K=1/12 ML
2	t_B, same row	-1.73	3.17	1.93	

Table 2: Calculated adsorption energies ($E_{ads,K}$) for one K atom on Co(11-20) with a pseudo step on within the (3x4) surface unit cell.

Adsorption geometry	$E_{ads,K}$ (eV)
offset t_B, beneath step	-2.18
t_B, away from step	-2.06

Table 3: Calculated adsorption energies ($E_{ads,CO}$) for one CO, and one CO co-adsorbed with one K on Co(11-20) within a (3x2) surface unit cell, CO bond length (d_{C-O}), the distance between K and nearest neighbor Co atom (d_{K-Co}), and the effective K radius (R_{eff}).

Adsorbate(s)	CO adsorption geometry	K adsorption geometry	$E_{ads,CO}$ (eV)	d_{C-O} (Å)	d_{K-Co} (Å)	R_{eff} (Å)
CO	b_A		-1.60	1.19		
	t_A		-1.59	1.17		
CO+ K	b_A	t_B	-1.93	1.22	3.36	2.12
	$b_{AB(1)}$	t_B, offset	-1.89	1.25	3.40	2.16
	t_A	t_B	-1.78	1.19	3.27	2.03